

# Through-thickness permeability modelling of woven fabric under out-of-plane deformation

Xueliang Xiao<sup>1\*</sup>, Andrew Long<sup>2</sup>, Xuesen Zeng<sup>2</sup>

<sup>1</sup> Institute of Textiles and Clothing, The Hong Kong Polytechnic University, Hung Hom, Hong Kong;

<sup>2</sup> Division of Materials, Mechanics and Structures, Faculty of Engineering, University of Nottingham, University Park, Nottingham, NG7 2RD, UK)

**Abstract:** When a woven fabric is subject to a normal uniform loading, its properties such as tightness and through-thickness permeability are both altered, which relates to the fabric out-of-plane deformation (OPD) and dynamic permeability (DP). In this article, fabric OPD is analytically modelled through an energy minimization method, and corresponding fabric DP is established as the function of loading and fabric deformed structure. The total model shows the permeability a decrease for tight fabric and an increase for loose fabric when the uniform loading increases. This is verified experimentally by fabric OPD, static and dynamic permeabilities. Experimental tests for both permeabilities showed good agreement with the corresponding predictions, indicating the fact that tight fabric becomes denser and loose fabric gets more porous during OPD. A sensitivity study showed that an increase of fabric Young's modulus or a decrease of fabric test radius both lead to an increase of DP for tight fabric and opposite for loose fabric. The critical fabric porosity and thickness were found for inflection of fabric DP trend during the OPD, which contributes to the optimum design of interlacing structure applied to protective textiles and composites.

**Keywords:** Analytical model; out-of-plane; permeability; uniform loading; woven fabric;

\*Corresponding author:

**Xueliang Xiao**, (✉)Email: [xiao\\_xueliang@163.com](mailto:xiao_xueliang@163.com) or [xueliang.xiao@polyu.edu.hk](mailto:xueliang.xiao@polyu.edu.hk)

(☎)Tel. +852 2766 5568

## 1 Introduction

Many technical textiles during bulking, such as inflation of airbag and artificial blood vessel, are subject to pressure loading perpendicular to the fabric in-planar. The perpendicular loading easily causes the interlacing structural fabric a deformed out-of-plane curved profile. The transient permeability and the subsequent protective effect and transport efficiency are thereafter varied dynamically during the deformation. Therefore, it is important to model this fabric out-of-plane deformation (OPD) behaviour and the relationship with the fabric dynamic permeability (DP), as the complete understanding of the mechanism from fabric OPD to fabric DP will be desirable for optimum design of such technical textiles and exploration of their new applications.

As known, 2D woven fabric is a flexible, discontinuous and anisotropic sheet, and can be easily deformed by an out-of-plane pressure load, which may involve fabric nonlinear tensile, shear, bending and compression behaviours. Hursa [1] used a fabric unit-cell geometrical model to predict the OPD with its micromechanical tensile, which may contribute to the link of fabric deformation to DP. King [2] proposed a continuum constitutive model for predicting fabric mechanical behaviour in planar direction. The approach relied on the selection of a geometrical model for the fabric weave, coupled with constitutive models for the yarn behaviours. The structural configuration was related to the macroscopic deformation through an energy minimization method. This method is useful as it covers all aspects of mechanical properties in the fabric OPD. Lin [3] developed an analytical model for the OPD of a square textile composite by its own weight. Trigonometric functions were used to describe the in-plane and out-of-plane displacements of any point. Energy minimization approach was employed to analyse the composite tensile, shear, bending and exerted external force. The predictions for the maximum deflections of a few weave composites showed good agreement with corresponding finite element simulations.

Table 1 Transverse permeability ( $K_{\perp}$ ) of yarns developed by a few researchers

Researcher	Hexagonal	Quadratic
Gebart [4] Eq.2	$K_h = \frac{16}{9\pi\sqrt{6}} \left( \sqrt{\frac{\pi}{2\sqrt{3}V_f}} - 1 \right)^{2.5} \cdot R_f^2$	$K_q = \frac{16}{9\pi\sqrt{2}} \left( \sqrt{\frac{\pi}{4V_f}} - 1 \right)^{2.5} \cdot R_f^2$
Cai [5] Eq.3	$K_h = 0.07R_f^2 \cdot \left( \frac{1 - \sqrt{\frac{V_f}{0.907}}}{\frac{V_f}{0.907}} \right)^{2.5}$	$K_q = 0.12R_f^2 \cdot \left( \frac{1 - \sqrt{\frac{V_f}{0.785}}}{\frac{V_f}{0.785}} \right)^{2.5}$
Bruschke [6] Eq.4	$K_h = \frac{R_f^2 (1-l^2)^2}{3\sqrt{3} l^3} \cdot \left( 3l \frac{\arctan\left(\frac{1+l}{\sqrt{1-l}}\right)}{\sqrt{1-l^2}} + \frac{l^2}{2} + 1 \right)^{-1}$ $l^2 = \frac{2\sqrt{3}(1-\Phi)}{\pi}$	$K_q = \frac{R_f^2 (1-l^2)^2}{3 l^3} \cdot \left( 3l \frac{\arctan\left(\frac{1+l}{\sqrt{1-l}}\right)}{\sqrt{1-l^2}} + \frac{l^2}{2} + 1 \right)^{-1}$ $l^2 = \frac{4(1-\Phi)}{\pi}$
Westhuizen [7] Eq.5	$K = R_f^2 \cdot \frac{\pi(1-V_f^*) \left(1 - \sqrt{V_f^*}\right)^2}{24(V_f^*)^{1.5}}$	$V_f^* = 2.22(V_f)^2 - 1.22V_f + 0.56 \quad (V_f \geq 0.5)$ $V_f^* = V_f \quad (V_f < 0.5)$

Fabric permeability ( $K$ ) is a measure of the fabric ability to transmit fluids and determined by the fabric geometrical parameters, such as porosity ( $\Phi$ ), fibre radius ( $R_f$ ) and fabric thickness ( $L$ ). For tight fabric under a certain pressure drop, fluid has to flow through the space around fibers in overlapping yarns. Hence the fabric permeability can be viewed as equivalent of its yarn permeability. Fiber volume fraction ( $V_f$ ),  $R_f$  and fiber array (usually hexagonal and quadratic) are the key factors in characterizing the yarn permeability. Table 1 gives a few analytical models for the relationship of  $K$  and the above geometric parameters, where  $K$  means a static value based on a specific fabric structure. In Table 1, Eq.3 is for an equivalent homogeneous medium based on a self-consistent approach while Eq.4 and Eq.2 are from lubrication solution. Eq.4 suits for high porous materials but Eq.2 handles high dense media. In addition, Eq.2 expresses fluid flow through unidirectional multi-filaments with circular cross-section but Eq.5 describes flow through filaments with square cross-section. Herein Eq.2 is selected for predicting the transverse permeability of fibre bundles in this article. Moreover, Gebart developed one more equation for flow along unidirectional fibres ( $K_{\parallel}$ ):

$$K_{\parallel} = \frac{8R_f^2 (1-V_f)^3}{c V_f^2} \quad (6)$$

Value for  $c$  is 57 when fibre array is quadratic and 53 for hexagonal. However, yarns are undulated in fabric, as shown in Fig.1(a), leading to the increased fabric permeability. Advani [8] introduced an expression (Eq.7) according with this situation:

$$K = K_{\parallel} \sin^2 \alpha + K_{\perp} \cos^2 \alpha - \frac{(K_{\perp} - K_{\parallel})^2 \cos^2 \alpha \sin^2 \alpha}{K_{\parallel} \cos^2 \alpha + K_{\perp} \sin^2 \alpha} \quad (7)$$

Where  $\alpha$  is the maximum crimp angle between the yarn axis and the in-plane direction of fabric as shown in Fig.1,  $K_{\parallel}$  and  $K_{\perp}$  are the permeabilities along (Eq.6) and perpendicular (Eq.2) to the fibre axis respectively. Eq.7 shows an increase of  $\alpha$  leads to the total fabric permeability increase, as shown a calculation example in Fig.1(b).

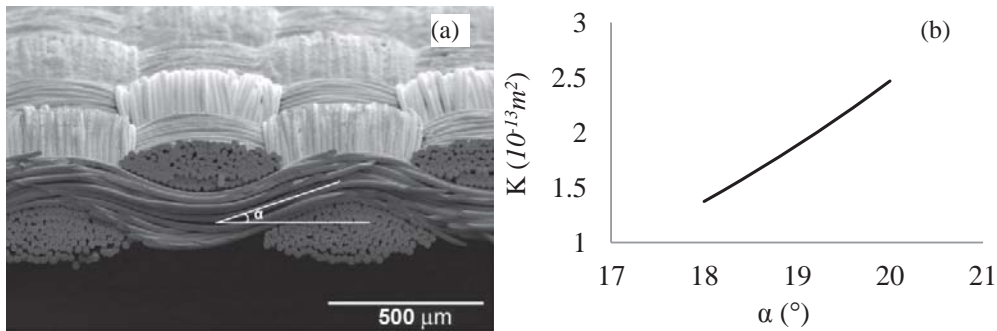


Figure 1 (a) cross-section of tight fabric, (b) relationship of permeability ( $K$ ) and crimp angle ( $\alpha$ )

For loose fabric with clear gaps between yarns, majority of fluid would flow through the gaps under a certain pressure drop. Gap radius ( $R_g$ ), yarn width ( $R_y$ ), fabric thickness ( $L$ ) and shape factor of flow channel ( $\lambda$ ) determine

the fabric permeability. Kulichenko [9] developed an analytical model for flow through the gaps assuming the gaps are parallel capillaries. Without  $\lambda$ , the model gives more than 60% error compared with the experimental fabric permeability. Xiao and Long [10] developed an analytical model for the static through-thickness permeability of woven fabric based on the work of Gebart [4], Phelan [11] and Kulichenko [9]. By defining  $R_g$  and  $R_y$  within hydraulic diameter,  $\lambda$  by a parabolic equation, there are:

$$R_g = \frac{(C_j - D_j)(C_w - D_w)}{C_j - D_j + C_w - D_w} \quad (8a)$$

$$R_y = \frac{C_j C_w}{C_j + C_w} - R_g \quad (8b)$$

$$y = \frac{x^2}{\lambda R_y} \quad (8c)$$

Where  $D_w$  and  $D_j$  are the widths of weft and warp yarns, while  $C_w$  and  $C_j$  are the spacings of weft and warp yarns respectively. A simplified diagram for this model is shown in Fig.2.

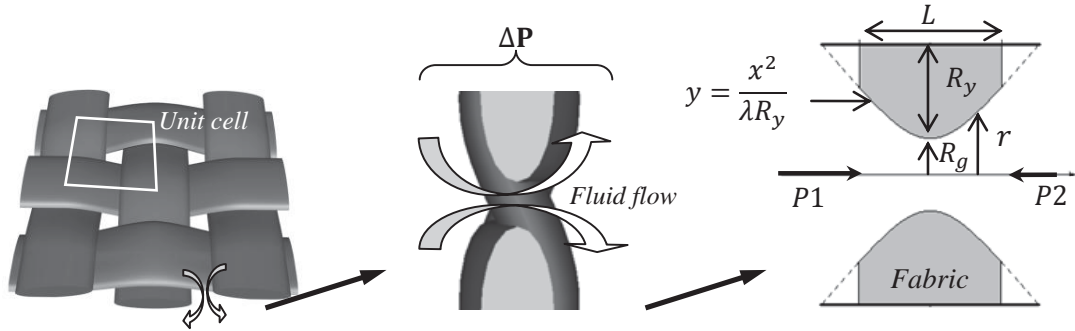


Figure 2 Parabola for boundary shape of flow channel between two yarns in a unit cell of woven fabric

This model was developed based on the Poiseuille flow theory and can be used for static permeability prediction for fabrics with clear gaps between yarns, i.e. loose fabrics. It was shown a close prediction with less than 15% error compared with experimental data:

$$K = \frac{2R_g^4}{5\pi} \frac{L}{\sqrt{\lambda R_g R_y (R_g + R_y)^2}} \quad (9)$$

This paper takes into account the fabric deformation under out-of-plane uniform loading (OPUL), and the effect on the fabric geometric parameters. The fabric DP is thereafter calculated based on the varying geometrical factors. Two typical fabrics (tight and loose) are used to make the experimental verifications. Results and discussions are given, following with the conclusions finally.

## 2 Analytical Modelling

### 2.1 fabric deformation under OPUL

Fabric behaviour under OPUL is modelled through assuming an originally flat, stress-free circular fabric sample with axisymmetric deformation. Polar coordinates are used in this particular deflection case.

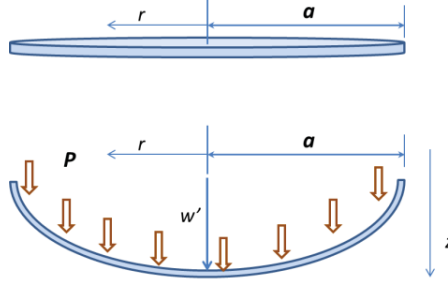


Figure 3 Schematic of geometry and polar coordinates for a deformed circular fabric

Fig.3 is the schematic diagram of a clamped circular fabric at free-state and its deflection under loading by side view. The origin of polar coordinates is placed at the centre of the fabric, giving the fabric radius  $a$ .  $r$  and  $z$  represent in-plane and out-of-plane directions. The boundary conditions in this case are:

$$r = 0, u = 0; r = a, u = 0; \quad (10a)$$

$$r = 0, w = w', \frac{dw}{dr} = 0; r = a, w = 0; \quad (10b)$$

Where  $u$  and  $w$  are the displacements in  $r$  and  $z$  direction respectively,  $w'$  is the maximum displacement in  $z$  direction. Due to the symmetric geometry and the uniform loading, it can be concluded that  $w$  is an even function of  $r$  whereas  $u$  is an odd function of  $r$ . The requirements can be satisfied by taking the following trigonometric approximations for the displacements:

$$u = c \cdot \sin\left(\frac{\pi r}{a}\right) \quad (11a)$$

$$w = w' \cos\left(\frac{\pi r}{2a}\right) \quad (11b)$$

Where  $c$  is an arbitrary constant. Note that the shape of Eq.11 is different with the approximation Eq.12 which exhibits less gradual deflection near the edge of clamped area [12], which is suitable for a continuous and rigid deformed sheet:

$$w = w' \left(1 - \frac{r^2}{a^2}\right)^2 \quad (12a)$$

$$u = r(a - r)(c_1 + c_2 r) \quad (12b)$$

Where  $c_1$  and  $c_2$  are factors depending on the boundary conditions. Similarly with Eq.12, the modelling of the fabric deflection reduces to derivation of the coefficients  $c$  and  $w'$  in Eq.11. The coefficients can be determined by the principle of virtual displacements. Under the OPUL, three types of fabric energy occur during the deformation:

bending energy  $U_b$ , strain energy  $U_m$  and loading work done  $W$ . Bending energy ( $U_b$ ) in polar coordinates is defined as:

$$U_b = \frac{\mathbf{D}}{2} \iint_0^A \left\{ \left( \frac{\partial^2 w}{\partial r^2} + \frac{1}{r} \frac{\partial w}{\partial r} + \frac{1}{r^2} \frac{\partial^2 w}{\partial \theta^2} \right)^2 - 2(1-\nu) \frac{\partial^2 w}{\partial r^2} \left( \frac{1}{r} \frac{\partial w}{\partial r} + \frac{1}{r^2} \frac{\partial^2 w}{\partial \theta^2} \right) + 2(1-\nu) \left( \frac{1}{r} \frac{\partial^2 w}{\partial r \partial \theta} - \frac{1}{r^2} \frac{\partial w}{\partial \theta} \right)^2 \right\} r dr d\theta \quad (13)$$

Where  $A$  is the test area,  $\nu$  is the Poisson's ratio. The Eq.13 for the deformed circular fabric can be reduced to a simple form due to the axisymmetric bending:

$$U_b = \pi \mathbf{D} \int_0^a \left\{ \left( \frac{\partial^2 w}{\partial r^2} + \frac{1}{r} \frac{\partial w}{\partial r} \right)^2 - \frac{2(1-\nu)}{r} \frac{dw}{dr} \frac{\partial^2 w}{\partial r^2} \right\} r dr \quad (14)$$

Where  $\mathbf{D}$  is the fabric flexural rigidity, which does not equal to  $\frac{EL^3}{12(1-\nu^2)}$  for fabric [3] where  $E$  is the fabric Young's modulus. This is due to the fact that the multi-filament structure in fabric bending does not have a mid-plane where its inside is compressed and outside is stretched.

Fabric strain energy ( $U_m$ ) consists of stretching energy and shearing energy, which plays a pivotal role in the fabric deformation. The expression in polar coordinates is given [12]:

$$U_m = \frac{\pi EL}{1-\nu^2} \int_0^a \{ \varepsilon_r^2 + \varepsilon_\theta^2 + 2\nu \varepsilon_r \varepsilon_\theta \} r dr \quad (15)$$

Where  $\varepsilon_r$ ,  $\varepsilon_\theta$  are the radial and tangential normal strains. The relationships of strains and displacements are:

$$\varepsilon_r = \frac{du}{dr} + \frac{1}{2} \left( \frac{\partial w}{\partial r} \right)^2 \quad (16a)$$

$$\varepsilon_\theta = \frac{u}{r} \quad (16b)$$

By substitution of Eq.16 into Eq.15, the expression of  $U_m$  is obtained in the form:

$$U_m = \frac{\pi EL}{1-\nu^2} \int_0^a \left\{ \left( \frac{du}{dr} \right)^2 + \frac{du}{dr} \left( \frac{dw}{dr} \right)^2 + \frac{u^2}{r^2} + \frac{2\nu u}{r} \frac{du}{dr} + \frac{\nu u}{r} \left( \frac{dw}{dr} \right)^2 + \frac{1}{4} \left( \frac{dw}{dr} \right)^4 \right\} r dr \quad (17)$$

Where the component expression  $\left( \frac{\pi EL}{1-\nu^2} \int_0^a \left( \frac{2\nu u}{r} \frac{du}{dr} + \frac{\nu u}{r} \left( \frac{dw}{dr} \right)^2 \right) r dr \right)$  represents shearing energy and the rest is stretching energy.

When the fabric undergoes OPUL, the work done ( $W$ ) by the loading  $P$  per unit area on the fabric from the initial to the equilibrium state is expressed by integrating  $Pw$  across the area of the fabric as:

$$W = \iint_0^A Pw dx dy \quad (18a)$$

$$W = 2\pi \int_0^a wPr dr \quad (18b)$$

Therefore the potential energy function ( $U_{\Pi}$ ) for the clamped fabric under an OPUL contains the bending energy, the strain energy and the work done:

$$U_{\Pi} = U_b + U_m - W \quad (19)$$

Where ‘-’ in Eq.19 represents an external energy to the fabric. In Eq.19,  $U_b$  relates to OPD;  $U_m$  links strain energy to the fabric Young’s modulus, which concerns with in-plane deformation;  $W$  denotes the work done by the uniformly distributed loading.

With the assumed deflected fabric shape (Eq.11), the first order and the second order of derivatives with respect to  $r$  are:

$$\frac{du}{dr} = \frac{\pi c}{a} \cos \frac{\pi r}{a} \quad (20a)$$

$$\frac{dw}{dr} = -\frac{\pi w'}{2a} \sin \frac{\pi r}{2a} \quad (20b)$$

$$\frac{d^2w}{dr^2} = -\frac{\pi^2 w'}{4a^2} \cos \frac{\pi r}{2a} \quad (20c)$$

By substituting Eq.20 into Eq.14 and Eq.17 then integrating over the clamped fabric as well as Eq.18, the results are:

$$U_b = \frac{\pi^3 D w'^2}{4a^2} \left( \frac{\nu \pi}{2a} + \ln \frac{\pi}{2} \right) \quad (21a)$$

$$U_m = \frac{\pi E L}{1-\nu^2} \left( \frac{\pi^2 c^2}{4} - \frac{\pi c w'^2}{4a} - \frac{c w'^2 \pi^3}{32a} + \frac{\nu c \pi w'^2}{3a} + \frac{\pi^2 w'^4}{64a^2} + \frac{3\pi^4 w'^4}{1024a^2} + \frac{c^2}{2} \ln 2 \right) \quad (21b)$$

$$W = 4 \left( 1 - \frac{2}{\pi} \right) P w' a^2 \quad (21c)$$

In Eq.21b, the condition  $\frac{\partial U_m}{\partial c} = 0$  that can make  $U_m$  a minimum that leads to:

$$c = \left( \frac{3\pi w'^2 - 4\nu \pi w'^2}{12a} + \frac{\pi^3 w'^2}{32a} \right) / \left( \frac{\pi^2}{2} + \ln 2 \right) \quad (22)$$

Inserting Eq.22 and Eq.21 into Eq.19 with a numerical calculation:

$$U_{\Pi} = \frac{0.52 + \nu - 0.3\nu^2}{1-\nu^2} \frac{E L w'^4}{a^2} + \frac{(2.8344 + 3.87\nu) D w'^2}{a^2} - 1.4535 P w' a^2 \quad (23)$$

Then, application of the minimization theory,  $\frac{\partial U_{\Pi}}{\partial w'} = 0$ , yields approximate expressions for the maximum deflection ( $w'$ ) and out-of plane displacement ( $w$ ) in the forms:

$$w' \cong a \cdot \sqrt[3]{\frac{1.4535 P a}{E L} \cdot \frac{1-\nu^2}{2.08 + 4\nu - 1.2\nu^2}} \quad (24a)$$

$$w = a \cdot \sqrt[3]{\frac{1.4535Pa}{EL} \cdot \frac{1-\nu^2}{2.08+4\nu-1.2\nu^2} \cdot \cos\left(\frac{\pi r}{2a}\right)} \quad (24b)$$

It is noted that, here fabric has been viewed as a flexible thin film as the  $w'$  value is much greater than the fabric thickness. In this condition, the resistance of the film to bending is negligible and the  $U_b$  can be ignored compared with the  $U_m$  in calculation.

## 2.2 Permeability of the deformed fabrics

Eq.24 can predict the fabric  $w'$  under a certain uniform load. The corresponding length of the deflected profile ( $l$ ) is integrated across a diameter:

$$l = \int_{-a}^a \sqrt{1 + (f'(w))^2} dr \quad (-a \leq r \leq a) \quad (25)$$

Where the  $f'(w)$  is the derivative of  $f(w)$  with respect to  $r$ . The strain ( $\varepsilon$ ) along the diameter is calculated:

$$\varepsilon = \frac{l-2a}{2a} \quad (26)$$

All yarns are assumed with the same  $\varepsilon$  value in the deformation.

### 2.2.1 Tight fabric permeability

Yarn cross-section in the tight fabric is assumed lenticular with width  $D$  and height  $h$  as shown a tight fabric cross-section in Fig.1a. Fig.4 simulates the change of tight fabric cross-section during OPD.

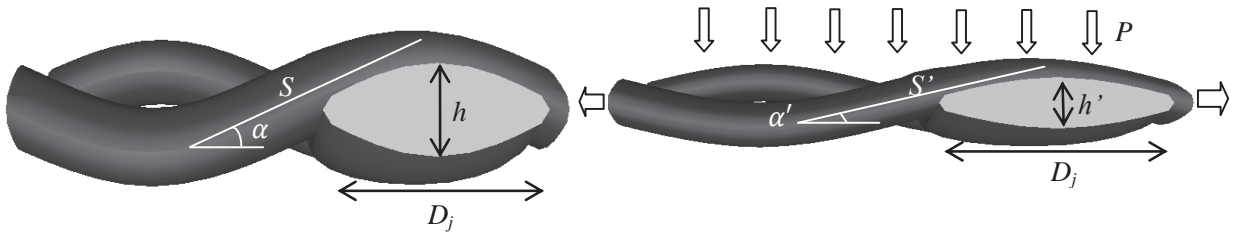


Figure 4 Geometrical change of fabric cross-section under uniform loading

During the OPD,  $R_f$  and  $D$  are supposed to be invariable, the  $h$  is reduced into  $h'$ , as shown in Fig.4, which has an assumed relationship under a yarn Poisson's ratio 0.5:

$$h' = \frac{h}{1+\varepsilon} \quad (27)$$

Where  $\varepsilon$  is based on Eq.26. Yarn  $V_f$  is defined as the total area of fibre cross-section divided by the area of yarn cross-section. Therefore, the original  $V_f$  value and its deformed value  $V_f'$  are expressed as:

$$V_f = \frac{nR_f^2}{Dh} \quad (28a)$$



$$V_f' = \frac{nR_f^2}{Dh'} \quad (28b)$$

Where  $n$  is the number of the filaments in a yarn. Then the relationship of  $V_f'$  and  $V_f$  should be:

$$V_f' = V_f(1 + \varepsilon) \quad (29)$$

For the crimp angle ( $\alpha$ ) in Fig.4, the values of  $\alpha$  and  $\alpha'$  are:

$$\sin \alpha = \frac{h}{s} \quad (30a)$$

$$\sin \alpha' = \frac{h'}{s(1+\varepsilon)} \quad (30b)$$

The relationship of the deformed  $\alpha'$  and the original  $\alpha$  is:

$$\sin \alpha' = \frac{\sin \alpha}{(1+\varepsilon)^2} \quad (31)$$

Substitution of the parameters  $V_f'$  and  $\alpha'$  into Eqs.2, 6 & 7 allows the permeability of the deformed tight fabric to be predicted theoretically.

### 2.2.2 Loose fabric permeability

For the deformed loose fabric, the yarn cross-section is assumed elliptical, the yarn width is also assumed constant. During OPD, the yarn height is decreased while the yarn length is increased with  $\varepsilon$  under yarn Poisson's ratio 0.5 (refer to Eq.27). The enlarged  $R_g'$  between yarns is calculated as follows due to the stretched yarn length with  $\varepsilon$ :

$$R_g' = R_g(1 + \varepsilon) \quad (32)$$

The shape factor ( $\lambda$ ) of the flow channel (gap between yarns) in Eq.9 relates to the fabric thickness ( $L$ ):

$$\lambda' = \frac{\lambda}{(\frac{L}{L'})^2} = \frac{\lambda}{(1+\varepsilon)^2} \quad (33)$$

Substitution of the parameters  $R_g'$ ,  $h'$  and  $\lambda'$  into Eq.9 allows the permeability of the deformed loose fabric to be predicted theoretically.

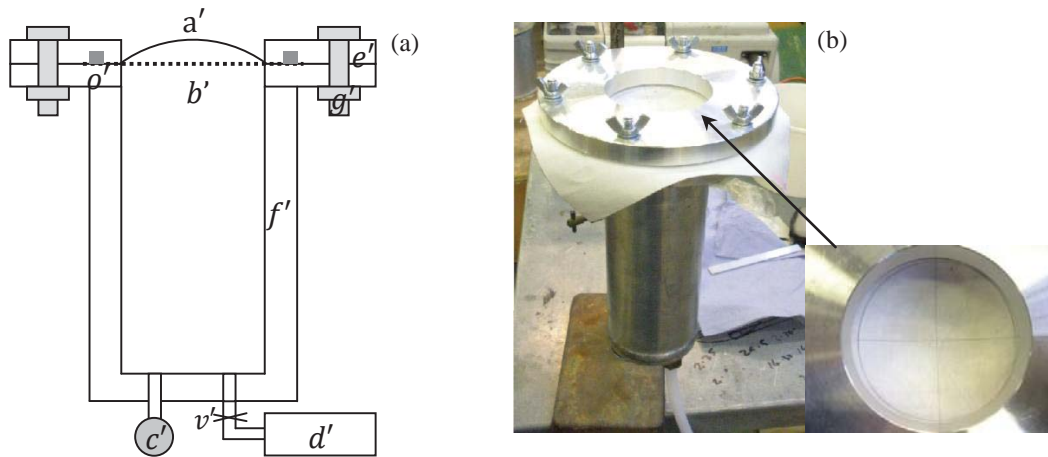
## 3 Experimental verification

### 3.1 Fabric deformation model

The experimental verification to the model of fabric OPD contains two aspects: the  $w'$  and corresponding  $w$ . Here a novel experimental device is invented to validate the deformation model.

1  
2  
3  
4 *3.1.1 Design of the fabric deflection tester*  
5  
6

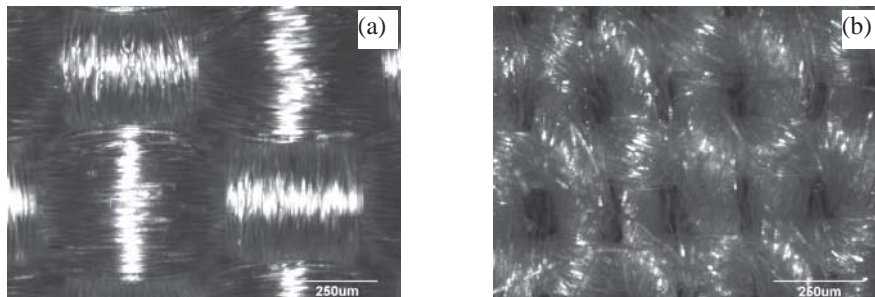
7 Fig.5 shows the design of the fabric deflection tester. In Fig.5a, a stress-free flat fabric (*b'*) is clamped by two plates (*e'*) with six bolts (*g'*). The fabric edge is sealed by a compressed rubber ring (*o'*) in plates. The testing diameter of the fabric in this device is 82 mm. A larger of cling film (*a'*) is in place to ensure the system is airtight. The size of the film is slightly greater than that of the fabric to avoid influence on fabric deformation. The air in the container (*f'*) is pumped by a vacuum pump (*d'*). There is a valve (*v'*) that can control the vacuum level in the container. A vacuum pressure gauge (*c'*) gives the pressure reading inside the sealed container.  
8  
9  
10  
11  
12  
13  
14  
15



32 Figure 5 Fabric deflection tester: (a) construction sketch; (b) real tester  
33

34 The device is designed to produce a vacuum pressure up to 100 KPa. A steel ball with diameter of 4 mm is used to determine the place of *w'*. A ruler is placed on the top plate across a diameter parallel to the fabric warp, weft and 45° of warp/weft directions respectively. A vernier caliper is placed on the ruler perpendicularly and movable to determine the displacement of the fabric deflection. Each fabric deflection under a certain pressure load was repeated five times for the three directions with a fresh sample. Average fabric deflections for the repeats were given with standard deviations.  
35  
36  
37  
38  
39  
40  
41  
42  
43

44  
45 *3.1.2 Experimental materials*  
46



58 Figure 6 Fabric structure of (a) Fabric A<sub>1</sub>; (b) Fabric U<sub>2</sub>  
59  
60  
61  
62  
63  
64  
65

The top views of two woven fabrics are shown in Fig.6 and their specifications are listed in Table 2. The fabric  $L$  was determined using the FAST-1 (Fabric Assurance by Simple Testing) device developed by CSIRO. A **compression** pressure of  $196 Pa$  was applied to the fabric during the measurement [13]. Fabric images were obtained using a ZEISS AxioScope A1 microscope. The images were used to measure  $C$  (distance between yarn centre lines),  $D$  and  $\alpha$  by a free image analysis software Image-J [14]. It is noted that Fabric  $A_1$  represents a tight fabric with no gaps between yarns. The yarns in Fabric  $A_1$  are made of multi-filaments without any twist. In contrast, Fabric  $U_2$  is a loose fabric with clear gaps. The yarns in this fabric are made of 65% PET and 35% cotton staple fibres, which are ‘Z’ spinning with twist of  $858/m$ .

Table 2 Fabric specifications **in average values** before OPUL ( $\pm$  Standard Deviation)

Fabric	Composition and structure	$R_f$ <i>mm</i>	Yarn $V_f$	$L$ <i>mm</i>	$\alpha$	$C$ <i>mm</i>		$D$ <i>mm</i>	
						Warp	Weft	Warp	Weft
$A_1$	100% Nylon plain	0.34 ( $\pm 0.01$ )	0.68 ( $\pm 0.01$ )	0.34 ( $\pm 0.01$ )	$20^\circ$	0.53 ( $\pm 0.02$ )	0.45 ( $\pm 0.01$ )	0.45 ( $\pm 0.01$ )	0.52 ( $\pm 0.01$ )
	Composition and structure		Ave $\lambda$						
$U_2$	65%PET/35% Cotton plain		12.96 ( $\pm 0.32$ )	0.32 ( $\pm 0.01$ )	$14^\circ$	0.22 ( $\pm 0.03$ )	0.33 ( $\pm 0.01$ )	0.17 ( $\pm 0.03$ )	0.19 ( $\pm 0.03$ )

Fabric Young’s modulus ( $E$ ) and flexural rigidity ( $\mathbf{D}$ ) were both measured by Kawabata Evaluation System (KES) [15]. Two parameters were both tested using samples with size  $30cm \times 20cm$ . In KES, one side of fabric was gripped by two fixed grippers paralleled to its warp or weft yarns while the other side was gripped by movable grippers. If the movable grippers stretch a fabric forward with an increasing load up to  $4.9 N$ , the increased tensile stress ( $N/mm$ ) and fabric strain (%) was recorded. Its slope divided by  $L$  (assumed constant) was the fabric  $E$  value with a unit  $Pa$ . In Fig.7, the slope of tensile stress-strain of Fabric  $A_1$  is almost a constant when the strain is less than 10%. However, the slope keeps increasing for Fabric  $U_2$ . The average values of initial  $E$  for warp and weft directions are calculated as  $247 MPa$  for Fabric  $A_1$  and  $148 MPa$  for Fabric  $U_2$  **when both stains are less than 10%**. If the movable grippers rotate around the fixed grippers with a sample, a relationship of bending moment and fabric curvature was recorded as a closed curve. Slope of the first part of the curve in Fig.7 is the  $\mathbf{D}$  value with a unit  $Nmm$ . The expression  $\frac{EL^3}{12(1-\nu^2)}$  was calculated as  $889 \times 10^{-6} Nm$  for Fabric  $A_1$  and  $444 \times 10^{-6} Nm$  for Fabric  $U_2$  based on the measurements of  $E$ ,  $L$  and  $\nu(0.5)$  for both fabrics, which are much larger than the corresponding measured  $\mathbf{D}$  values  $66.4 \times 10^{-6} Nm$  for Fabric  $A_1$  and  $7.85 \times 10^{-6} Nm$  for Fabric  $U_2$  from Fig.7. This proves that the equation  $\mathbf{D} = \frac{EL^3}{12(1-\nu^2)}$  for continuous solid plates does not suit for textile fabrics.

An attempt was made to measure  $\nu$  values of the two fabrics using Digital Image Correlation (DIC) equipment according to Hursa’s approach [16], however the results showed both larger than 1 which is not considered physically realistic. In the next section, a few  $\nu$  values will be used to assess sensitivity.

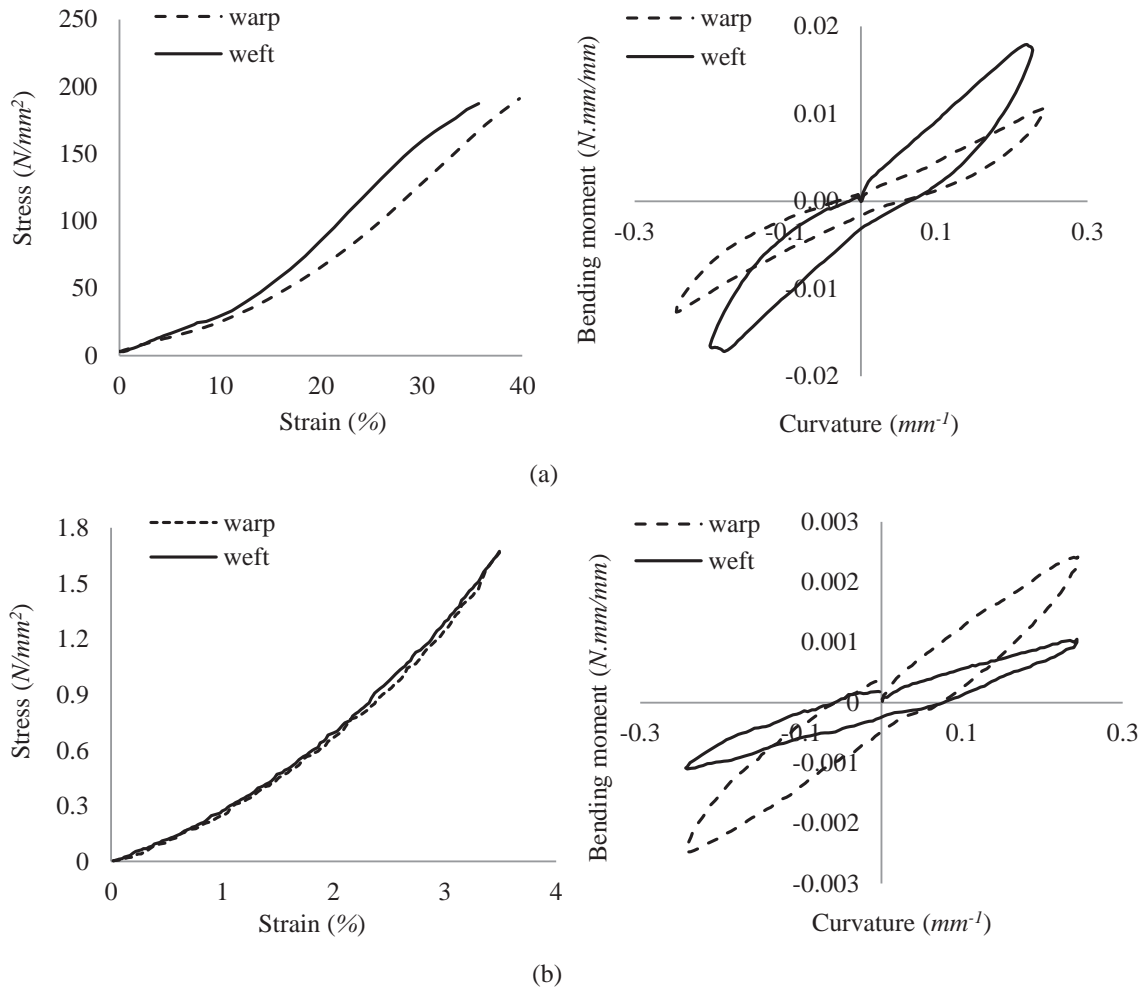


Figure 7 Tensile stress-strain and bending moment-curvature relationships of fabrics obtained by KES: (a) Fabric A<sub>1</sub>; (b) Fabric U<sub>2</sub>

### 3.2 Deformed fabric permeability measurement

The fabric through-thickness  $K$  without deformation was measured by a Shirley Air Permeability Tester. The air pressure drop is 300 Pa. The test area is 5.07 cm<sup>2</sup> (1 inch<sup>2</sup>) and the airflow rate is in the range of 0.1-350 cm<sup>3</sup>/s. Each fabric was tested five times. The  $K$  value was calculated according to Darcy's law:

$$\frac{P}{L} = \frac{\mu V}{K} \quad (34)$$

Where  $\mu$  is the gas viscosity and  $V$  is the average gas velocity. The fabric through-thickness  $K$  value during the OPD was measured by a 'dynamic permeability tester', which was designed and constructed by Leeds University. More details about the working principle of the tester can be found in Bandara [17] or Xiao [18]. The tester provides a circular test area of 50 cm<sup>2</sup>. The test pressure is in the range of 5 KPa and 300 KPa above atmospheric pressure. For

the two fabrics, the initial uniform loading of 80 KPa was applied. The  $K$  value was obtained by the Forchheimer equation:

$$\frac{P}{L} = \frac{\mu}{K}V + \beta\rho V^2 \quad (35)$$

Where  $\rho$  is the gas density,  $\beta$  is the non-Darcy coefficient.

## 4 Results and discussions

### 4.1 Fabric deformation model

#### 4.1.1 Maximum displacement

The maximum displacement ( $w'$ ) of fabric occurs at the centre of the test area under OPUL. The prediction is based on Eq.24a, assuming three  $\nu$  values (0.2, 0.3 & 0.4) in the range for woven fabric [16, 19]. The comparisons of  $w'$  between predictions ('Pred' curves) and measurements ('EXPT' dots) are shown in Fig.8.

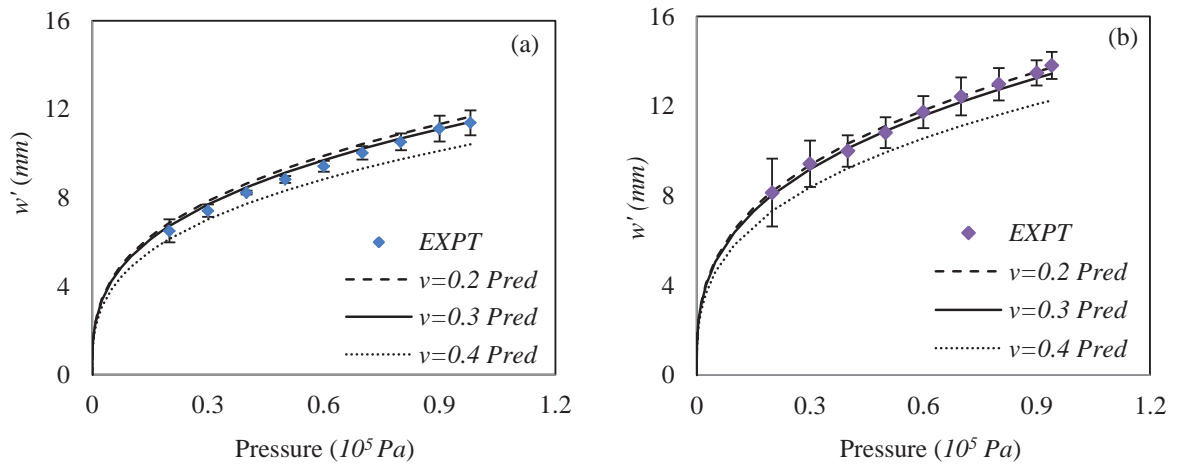


Figure 8 Fabric maximum displacements during out-of-plane uniform loading: (a) Fabric A<sub>1</sub>; (b) Fabric U<sub>2</sub>

With a fixed  $\nu$  value, the predicted  $w'$  is proportional to the cubic root of the OPUL ( $P$ ) according to Eq.24a. The 'EXPT' dots in Fig.8 show a nonlinear relationship of  $w'$  and  $P$  which is close to the cubic root relationship in the prediction. The graphs also show that a smaller  $\nu$  value can obtain a higher prediction of  $w'$ , and the interval between  $\nu = 0.2$  and 0.3 is much less than that of 0.3 and 0.4, showing the relationship of  $w'$  and  $\nu$  values is nonlinear. The comparisons show the  $\nu$  value for Fabric A<sub>1</sub> is close to 0.3 while Fabric U<sub>2</sub> is close to 0.2. In the graph, the  $w'$  value for Fabric A<sub>1</sub> is smaller than that for Fabric U<sub>2</sub> at the same loading. The reason is a smaller stiffness value of Fabric U<sub>2</sub>.

#### 4.1.2 Deflection profile

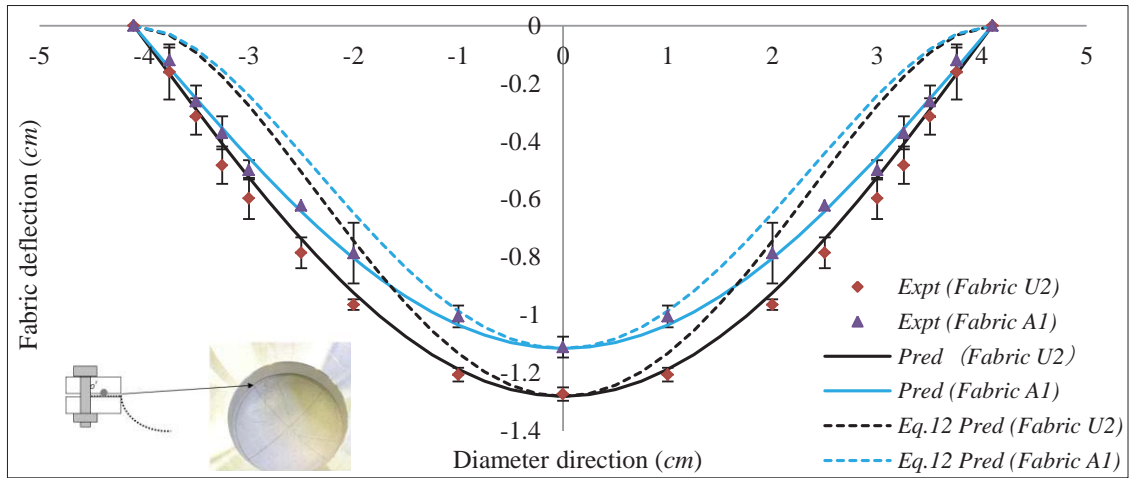


Figure 9 Comparison of experimental measurements against predictions of fabric deflection along diameter (Error bars represent standard derivation based on five repeats of tests at each point)

Fig.9 compares the experimental measurements of fabric deflection based on the average value for three directions along a diameter with the predictions based on Eq.11 and Eq.24b (the curves ‘Pred’ in Fig.9). The ‘Eq.12 Pred’ profile in Fig.9 is based on Eq.12 which assumes the displacement equations are polynomials. The fabric deflections in Fig.9 are both under the same uniform loading of 100 KPa, where the  $w'$  values are found of 1.1 cm for Fabric A<sub>1</sub> and 1.28 cm for Fabric U<sub>2</sub>. This gives the strain  $\epsilon$  values of 3.6% for Fabric A<sub>1</sub> and 6.6% for Fabric U<sub>2</sub> according to the Eqs.25 & 26. It is evidently practicable of the  $E$  values obtained from Fig.7 for the fabric deformation prediction. Here the  $\nu$  values for predictions are 0.3 for Fabric A<sub>1</sub> and 0.2 for Fabric U<sub>2</sub>. The experimental results prove the approximations (Eq.11) for the fabric deflection are reasonable and more accurate than that from Eq.12. The difference in the predictions based on between Eq.12 and Eq.11 is mainly displayed in the deflected profile near the clamped area. The prediction of Eq.12 show the vertical displacement declines slowly in this area due to the polynomial nature, and Eq.11 shows a steep deflection in contrast due to the cosine function.

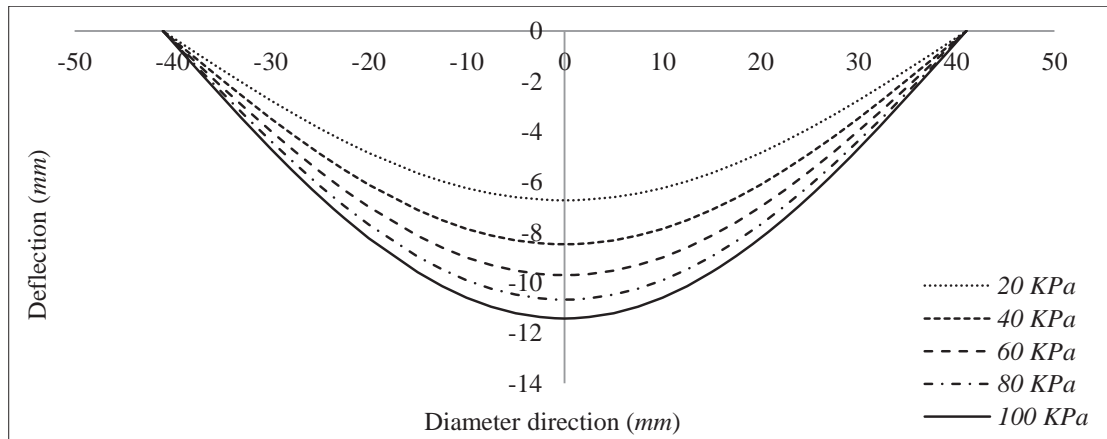


Figure 10 Deflection profiles of Fabric A<sub>1</sub> under different uniform loadings

Fig.10 shows the deflected profiles of Fabric A<sub>1</sub> along the same diameter under different OPULs. It is easier to deform at low loading due to the yarn crimp of interwoven structure of the woven fabric. A greater OPUL achieves less increased displacement because the loading is now undertaken by yarns in the in-plane direction.

#### 4.2 Permeability model of deformed fabric

##### 4.2.1 Tight fabric A<sub>1</sub>

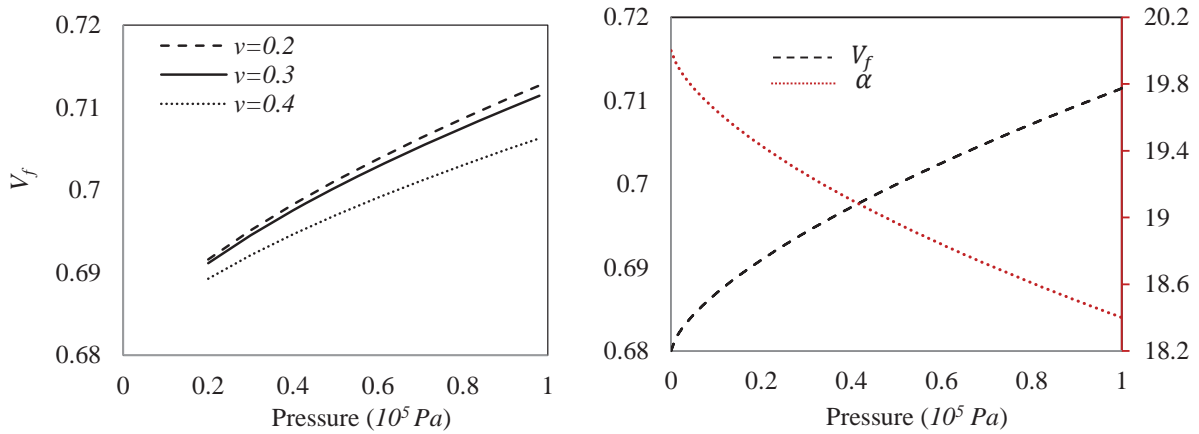


Figure 11 Effect of uniform loading on the parameters of  $V_f$  and  $\alpha$

Fig.11 shows the  $V_f$  and  $\alpha$  values are strongly influenced by OPUL. An increase in loading causes  $V_f$  to increase and  $\alpha$  to decrease. One reason might be the increased contact force at yarn cross-overs, which pushes fibres together in a tighter bundle. Fig.11 also shows a smaller  $\nu$  value causes yarns to exhibit a larger  $V_f$  value.

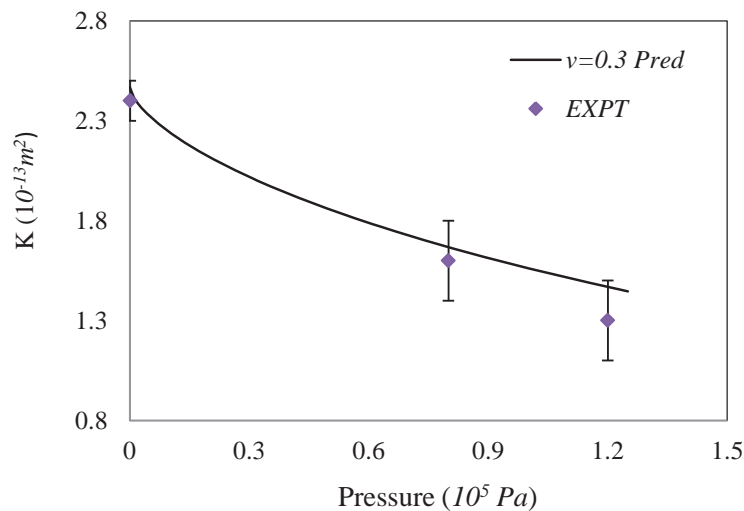


Figure 12 Comparison of permeability prediction with experimental data under increasing loadings

Fig.12 compares the fabric  $K$  prediction ( $\nu=0.3$ ) with experimental results under three OPULs. More details on experimental data processing can be found in Xiao's work [18]. The average tested values consist of one static and two dynamic permeabilities. As shown in Fig.12, the predictive model agrees with the experimental results very well. The  $K$  value is decreasing with the increase of OPUL for tight fabric. The essential reason is that  $V_f$  is increased due to the reduced  $h$  by increasing loading on fabric.

#### 4.2.2 Loose fabric $U_2$

Table 2 offers initial values of  $C$  and  $D$ , which can be transferred into  $R_g$  and  $R_y$  by Eq.8a&b. Due to the OPUL, the fabric deflection leads to an increase in the fabric surface area. Yarns tensioning causes an increase in  $R_g$  and a decrease in  $L$  and  $\lambda$ .

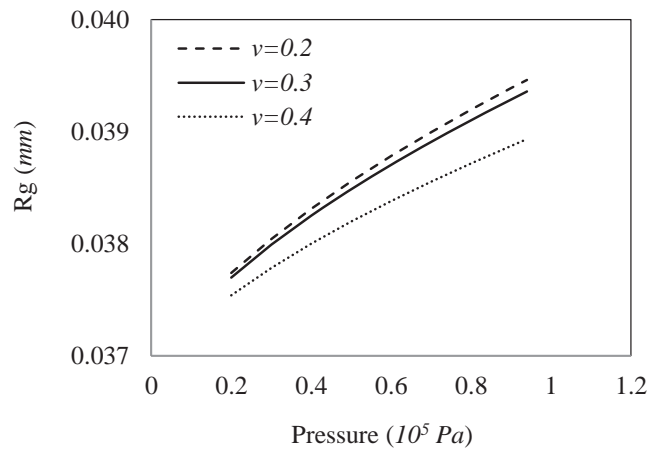


Figure 13 Effect of pressure load on  $R_g$

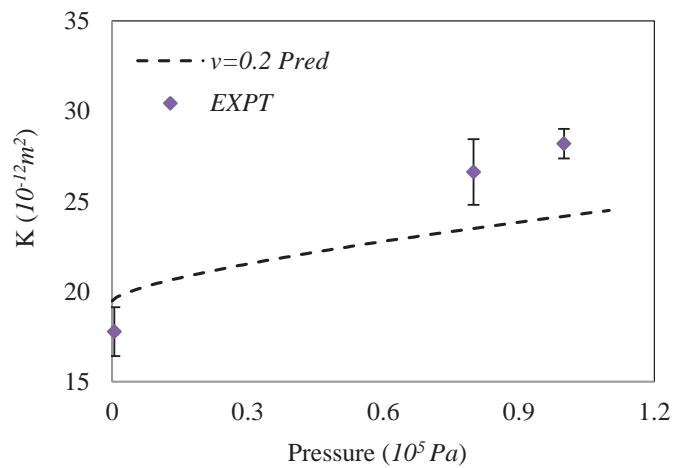


Figure 14 Comparison of permeability prediction and experimental values under increasing OPULs for Fabric  $U_2$



The similarity of Fig.13 with Fig.11 is due to the same basis of the Eqs.24-27. In Fig.13,  $R_g$  shows a nonlinear relationship with OPUL. An increase of the loading causes an increase of  $R_g$  from Eq.32. Substituting Eq.32 and Eq.33 into Eq.9,  $L$  and  $\lambda$  are eliminated, therefore there is no need to compare the effect of loading on the two geometrical factors  $L$  and  $\lambda$ . Fig.14 shows  $K$  is increasing as  $R_g$  is enlarged when the loading on the fabric increases. In the prediction, yarn permeability was ignored. The model predicts with reasonable accuracy for the relationship of permeability and loading in the test range. However, under the high OPUL, the model gives an underestimated prediction. The reason might be the limitation of Eq.9 as it was obtained from Darcy's law. The relationship of pressure drop and fluid velocity is nonlinear when the velocity reaches a particular high range. The Forchheimer equation (Eq.35) should be used for prediction of flow behaviour in this range.

#### 4.3 Sensitivity study

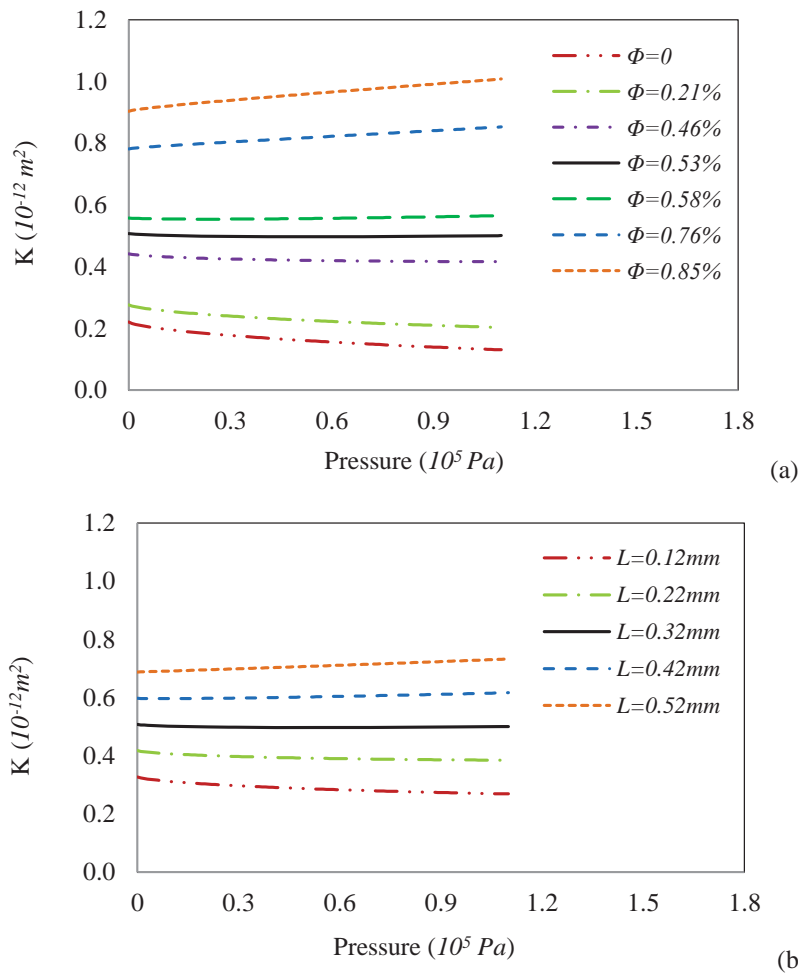


Figure 15 Effects of (a) original fabric porosity ( $\Phi$ ) and (b) original fabric thickness ( $L$ ) on the relationship of  $K$  and  $P$  (Fabric  $U_2$ )

The current model shows how to predict the through-thickness  $K$  of a woven fabric under certain OPUL. During the deformation,  $\Phi$  which is defined as the gap area divided by the fabric area, and  $L$  are the most sensitive parameters influenced by the loading. For loose fabric,  $K$  under the loading is increased due to the increase of  $\Phi$ . For tight fabric,  $K$  is reduced by decreasing  $L$ . Fig.15 investigates the sensitivity of  $\Phi$  and  $L$  to the  $K$  when fixing other specifications of Fabric U<sub>2</sub> under OPULs. Fig.15a shows the critical  $\Phi$  value is in the range of 0.5% and 0.6% which is much smaller than its original value 5.04% based on the specifications in Table 2. When  $\Phi$  is higher than 0.6%,  $K$  gets larger under OPULs. While  $\Phi$  is lower than 0.5%, the trend of  $K$  is opposite. When the  $\Phi$  value is 0.53% (critical value), increasing  $L$  gives a larger  $K$  value under the loading as shown in Fig.15b, and vice versa.

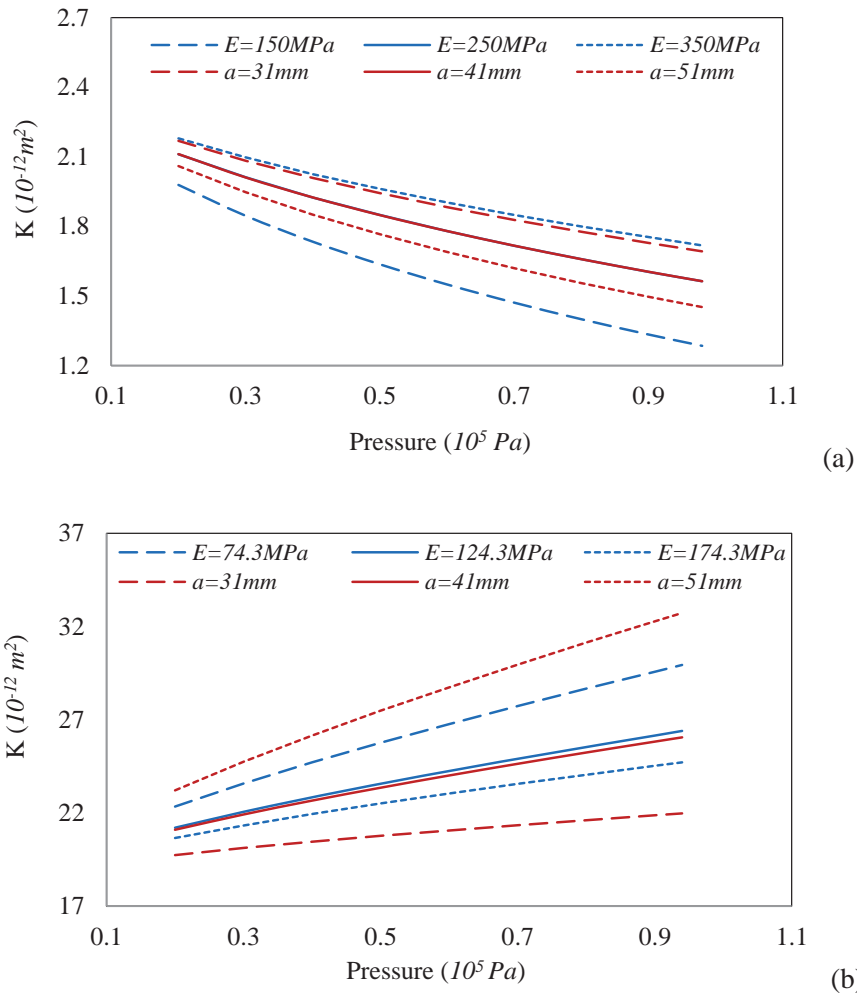


Figure 16 Effect of  $E$  and  $a$  on the relationship of  $K$  and  $P$ : (a) tight fabric; (b) loose fabric

Apart from  $\Phi$  and  $L$ , fabric  $E$ ,  $\nu$  and radius ( $a$ ) also relate to the final fabric  $K$  value. Herein, the effects of  $E$  and  $a$  on this relationship are discussed. Fig.16a shows an increase of  $E$  for tight fabric results in an increase of  $K$ . The reason is that the fabric deflection is decreased as  $E$  increases. Thereafter the yarn  $V_f$  decreases as discussed in Section 4.2.1 (Eq.29), leading to a higher  $K$ . However, the increase of  $K$  is nonlinear with the increase of  $E$ . It shows

1  
2  
3  
4  $K$  is decreased with an increase of loading for a fixed  $E$  value. In Fig.16b, loose fabric has the opposite trend  
5 compared with tight fabric. The  $R_g$  is increased as  $E$  is decreased, leading to a larger  $K$  value (Eq.9).  
6

7  
8 Fig.16 also shows the relationship by changing  $a$  when other parameters are fixed. An increase of  $a$  will increase the  
9  $w'$  value of the deformed fabric (Eqs.24) and  $\varepsilon$  value (Eqs.25 & 26), influencing the final  $K$  value. Fig.16a shows  
10 that  $K$  is decreased with increasing  $a$  as  $V_f$  is increased for tight fabric. The difference of  $K$  values between  $a =$   
11  $41\text{ mm}$  and  $a = 51\text{ mm}$  is smaller than that of  $a = 31\text{ mm}$  and  $a = 41\text{ mm}$ , indicating a lower effect of increased  
12  $a$  on decreasing the  $K$  value. Fig.16b shows  $K$  of loose fabric is increased as its  $a$  value increases. The reason might  
13 be that  $R_g$  is getting larger relatively as the fabric is deformed more at a larger  $a$  value. The difference of  $K$  values  
14 between  $a = 31\text{ mm}$  and  $a = 41\text{ mm}$  is smaller than that of  $a = 41\text{ mm}$  and  $a = 51\text{ mm}$ , indicating that an  
15 increase of  $a$  will cause the fabric  $K$  to increase further.  
16  
17  
18  
19  
20

## 21 **5 Conclusions**

22  
23  
24 Three analytical models were proposed for predicting the OPD of woven fabric under perpendicular uniform loading,  
25 and corresponding through-thickness permeability of tight weave and loose weave respectively. The whole models  
26 in this paper contribute to the mechanism understanding the effect of external factors on the fabric dynamic  
27 permeability, and assists with optimum design of technical textiles in the OPD working environment.  
28  
29  
30

31 In the modeling of fabric OPD under a uniform load, an energy-based approach was utilized to predict bending  
32 energy, strain energy and external energy. The fabric was assumed to behave like a thin film based on the membrane  
33 large deformation theory. Minimization energy of the system was used to derive the relationship of the maximum  
34 displacement and the loading. Fabric deflected shape was characterized by the displacement and a cosine function of  
35 the fabric radius. The model for predicting the permeability was based on the accurate prediction of the fabric  
36 deformation. Also it relied on the accurate prediction of the static permeability (Eqs.2, 6, 7, 8 & 9). The assumption  
37 was that the yarn width was invariable during the deformation. Fabric thickness was reduced with the same rate of  
38 yarn height. Tight fabric permeability was predicted through the increased yarn fibre volume fraction and crimp  
39 angle due to the decreased yarn height. Loose fabric permeability was predicted by the increased gap radius due to  
40 the enlarged fabric area caused by fabric deflection.  
41  
42  
43  
44  
45  
46

47 Three kinds of experiments were used to verify the analytical predictions. Fabric OPD was measured by a fabric  
48 deflection tester, with loading applied by a vacuum pump. Fabric static permeability was determined by a Shirley air  
49 permeability tester while fabric dynamic permeability was tested by a dynamic permeability tester. The predictions  
50 for the fabric deflection configurations (tight and loose fabrics) agree with the experimental measurements very well.  
51 The deflection causes the yarn fibre volume fraction and the crimp angle to increase, resulting in the permeability of  
52 tight fabric to decrease (Fig.12). In contrast, the deflection leads to the gap radius to increase, obtaining an increased  
53 permeability of loose fabric (Fig.14). The permeability predictions for the deformed fabrics agree with the  
54 experimental values well. Sensitivity studies firstly investigate the critical fabric porosity and the critical fabric  
55 thickness where the increase or decrease of fabric permeability occurs during the fabric deformation. Secondly the  
56  
57  
58  
59  
60  
61  
62

1  
2  
3  
4 fabric properties, such as Young's modulus, affect the fabric deformation. An increase of modulus leads to the  
5 increase of tight fabric permeability and a decrease of loose fabric permeability when the fabric is under the same  
6 pressure load.  
7  
8  
9

## 10 11 12 13 **Acknowledgements**

14  
15 The authors would like to thank Airbags International Ltd. for providing experimental materials, Leeds University  
16 and UK Unilever Resources Centre for undertaking the experimental tests.  
17  
18  
19  
20  
21

## 22 **Reference**

- 23  
24  
25 [1] Somodi Z, Rolich T, Hursa A (2010) Micromechanical tensile model of woven fabric and parameter  
26 optimization for fit with KES data, *Textile Research Journal*, 80(13): 1255-1264  
27  
28 [2] King MJ, Jearanaisilawong P, Socrate S (2005) A continuum constitutive model for the mechanical behavior of  
29 woven fabrics, *International Journal of Solids and Structures*, 42: 3867-3896  
30  
31  
32 [3] Lin H, Clifford MJ, Taylor PM, Long AC (2009) 3D mathematical modeling for robotic pick up of textile  
33 composites, *Composites: Part B*, 40: 705-713  
34  
35  
36 [4] Gebart BR (1992) Permeability of unidirectional reinforcements for RTM, *Journal of Composites Materials*,  
37 26(8): 1101-1133  
38  
39 [5] Cai Z, Berdichevsky AL (1993) An improved self-consistent method for estimating the permeability of a fiber  
40 assembly, *Polymer Composites*, 14(4): 314-323  
41  
42  
43 [6] Brusckke MV, Advani SG (1993) Flow of generalized Newtonian fluids across a periodic array of cylinders,  
44 *Journal of Rheology*, 37(3): 479-497  
45  
46  
47 [7] Westhuizen JV, Plessis JPD (1996) An attempt to quantify fibre bed permeability utilizing the phase average  
48 Navier-Stokes equation, *Composites: Part A*, 27A: 263-269  
49  
50  
51 [8] Advani SG, Brusckke MV, Parnas RS (1994) Resin transfer molding flow phenomena in polymeric composites,  
52 In 'Flow and rheology in polymer composites manufacturing', ed. S. G. Advani, Elsevier science B. V, Amsterdam.  
53  
54 [9] Kulichenko AV (2005) Theoretical analysis, calculation, and prediction of the air permeability of textiles, *Fibre*  
55 *Chemistry*, 37(5): 371-380  
56  
57  
58  
59  
60  
61  
62  
63  
64  
65

- 1  
2  
3  
4 [10] Xiao X, Zeng X, Long A, Clifford MJ, Lin H, Saldaeva E (2012) An analytical model for through-thickness  
5 permeability of woven fabric, *Textile Research Journal*, 82(5): 492-501  
6  
7  
8 [11] Phelan JF, Wise G (1996) Analysis of transverse flow in aligned fibrous porous media, *Composites: Part A*,  
9 27A (1): 25-34  
10  
11 [12] Ugural AC (1999) *Stresses in plates and shells* (2nd edition). Singapore: McGRAW HILL International editions.  
12 502.  
13  
14 [13] Boos AD, Tester D (1994) SiroFAST Fabric Assurance by Simple Testing, A system for fabric objective  
15 measurement and its application in fabric and garment manufacture; Available from: [www.tft.csiro.au](http://www.tft.csiro.au).  
16  
17  
18 [14] Image-J. 2012 [cited 2012 17/05]; Available from: <http://rsbweb.nih.gov/ij/features.html>.  
19  
20  
21 [15] Chan CK, Jiang XY, Liew KL, Chan LK, Wong WK, Lau MP (2006) Evaluation of mechanical properties of  
22 uniform fabrics in garment manufacturing. *Journal of Materials Processing Technology*, 174(1–3): 183-189.  
23  
24 [16] Hursa A, Rolich T, Razic SE (2009) Determining pseudo Poisson's ratio of woven fabric with a digital image  
25 correlation method. *Textile Research Journal*, 79(17): 1588-1598.  
26  
27 [17] Bandara P, Lawrence C, Mahmoudi M (2006) Instrumentation for the measurement of fabric air permeability at  
28 higher pressure levels, *Measurement science and technology*, 17: 2247-2255  
29  
30  
31 [18] Xiao X, Zeng X, Bandara P, Long A (2012) Experimental study of dynamic air permeability for woven fabrics,  
32 *Textile Research Journal*, 82(9): 920-930  
33  
34 [19] Lu Y, Dai X (2009) Calculation of fabrics Poisson's ratio based on biaxial extension. *Journal of Textile*  
35 *Research*, 30(9): 25-28  
36  
37  
38  
39  
40  
41  
42  
43  
44  
45  
46  
47  
48  
49  
50  
51  
52  
53  
54  
55  
56  
57  
58  
59  
60  
61  
62  
63  
64  
65